From Bulk to Monolayer MoS_2: Evolution of Raman Scattering

Hong Li, Qing Zhang, Chin Chong Ray Yap, Beng Kang Tay,* Teo Hang Tong Edwin, Aurelien Olivier, and Dominique Baillargeat*

Molybdenum disulfide (MoS_2) is systematically studied using Raman spectroscopy with ultraviolet and visible laser lines. It is shown that only the Raman frequencies of E^1_{2g} and A_{1g} peaks vary monotonously with the layer number of ultrathin MoS_2 flakes, while intensities or widths of the peaks vary arbitrarily. The coupling between electronic transitions and phonons are found to become weaker when the layer number of MoS_2 decreases, attributed to the increased electronic transition energies or elongated intralayer atomic bonds in ultrathin MoS_2. The asymmetric Raman peak at 454 cm^{-1}, which has been regarded as the overtone of longitudinal optical M phonons in bulk MoS_2, is actually a combinational band involving a longitudinal acoustic mode (LA(M)) and an optical mode (A_{2u}). Our findings suggest a clear evolution of the coupling between electronic transition and phonon when MoS_2 is scaled down from three- to two-dimensional geometry.

1. Introduction

Molybdenum disulfide (MoS_2) has a layered structure of hexagons that consist of covalently bonded Mo and S atoms. A plane of Mo atoms is sandwiched covalently between two planes of S atoms in a trigonal prismatic arrangement. Bulk MoS_2 is built up of S-Mo-S layers attached to each other through Van der Waals forces, and it is a good semiconducting material that can be employed for photovoltaic and photocatalyst applications.[1–3] In the past a few years, ultrathin MoS_2 flakes have been successfully obtained using the Scotch-tape method.[4] Field-effect transistors (FETs) based on monolayer MoS_2 have shown a field-effect mobility up to 200 $cm^2\ V^{-1}\ s^{-1}$ and a current on/off ratio of 10^8.[5] Theoretically, MoS_2 transistors could have even larger current on/off ratio (>10^{10}) and ideal subthreshold swing (60 mV dec^{-1}), and it is immune to the short-channel effect (drain-induced barrier lowing ~10 mV V^{-1}).[6] Moreover, strong photoluminescence has been detected in monolayer MoS_2 experimentally.[7,8] These superior optical and electronic properties make ultrathin MoS_2 attractive for low power optoelectronic applications. With rapid development of various ultrathin MoS_2-based devices, the unique property characterization and easy identification methods of atomic thick MoS_2 flakes are in high demand. Raman spectroscopy, a powerful nondestructive characterization tool, has been used to study different crystalline structures of MoS_2.[9–13] Off resonance, four first-order Raman active modes at 32 cm^{-1} (E^2_{2g}), 286 cm^{-1} (E_{1g}), 383 cm^{-1} (E^1_{2g}) and 408 cm^{-1} (A_{1g}) in bulk MoS_2 can be observed. The E^2_{2g} mode arises from the vibration of an S–Mo–S layer against adjacent layers. The E_{1g} mode is forbidden in back-scattering experiment on a basal plane. The in-plane E^1_{2g} mode results from opposite vibration of two S atoms with respect to the Mo atom while the A_{1g} mode is associated with the out-of-plane vibration of only S atoms in opposite directions.[14] On resonance, more Raman peaks are observed in bulk MoS_2 due to strong electron–phonon couplings. The most prominent mode around 460 cm^{-1} arises from a second-order process involving the longitudinal acoustic phonons at M point (LA(M)). Most of the new peaks are typically assigned to multiphonon bands involving LA(M) and other phonons at M point.[10,13] Very recently, Lee et al. reported on the layer thickness dependent E^1_{2g} and A_{1g} peak frequencies, intensities and widths in ultrathin MoS_2 flakes.[15] In contrast, we find that the Raman frequencies of E^1_{2g} and A_{1g} peaks, instead of the intensities and widths of the peaks, vary monotonously with the layer number of ultrathin MoS_2 flakes and can be used as reliable features to identify the layer number. In this paper, we present systematic Raman study of ultrathin MoS_2 flakes using various laser lines. With resonance Raman spectroscopy, the couplings between the electronic structure and phonons in ultrathin MoS_2 flakes are addressed.

Dr. H. Li, Prof. Q. Zhang, C. C. R. Yap, Prof. B. K. Tay
Microelectronics Centre
School of Electrical and Electronic Engineering
Nanyang Technological University
Singapore 639798, Singapore
E-mail: eqzhang@ntu.edu.sg; ebktay@ntu.edu.sg
Dr. T. H. T. Edwin, Dr. A. Olivier, Prof. D. Baillargeat
CINTRA, Research Techno Plaza
Nanyang Technological University
50 Nanyang Drive, Singapore 639798, Singapore

DOI: 10.1002/adfm.201102111

2. Results and Discussion

MoS_2 flakes were mechanically exfoliated from a piece of commercially available nature crystalline MoS_2 sample (SPI Supplies) with Scotch tape.[16] **Figure 1**a shows the optical image of a MoS_2 flake (sample S1) consisting of monolayer (1 L), bilayer

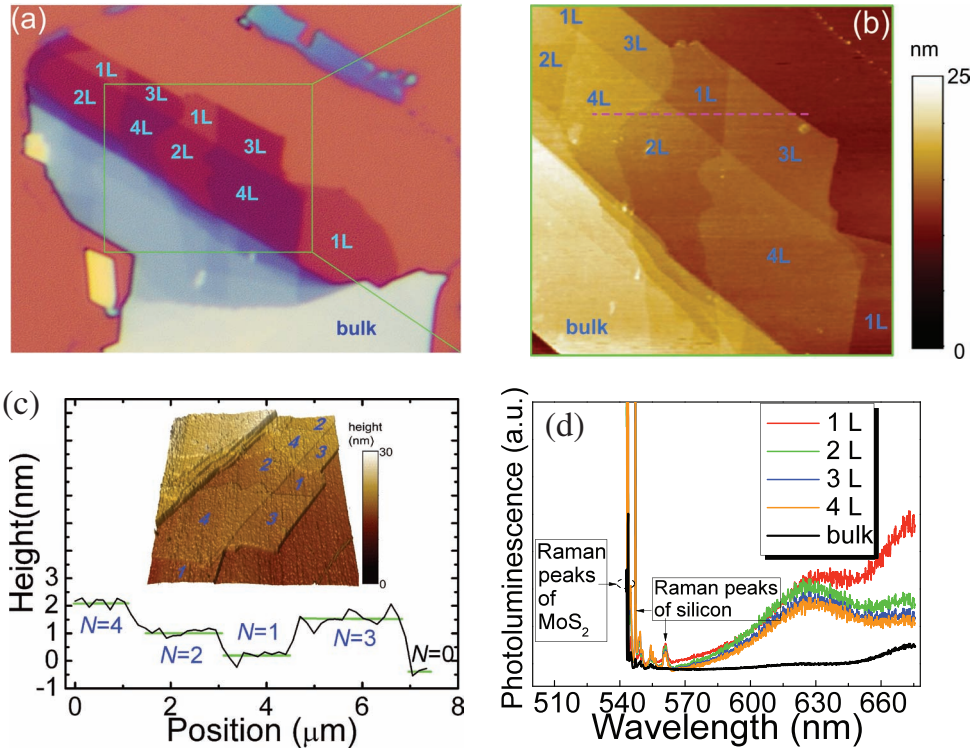

Figure 1. Optical image, AFM image and photoluminescence spectra of sample S1. a) Optical image of sample S1 placed on the surface of a heavily doped silicon wafer capped by 285-nm-thick silicon dioxide. The number of layers (1 L, 2 L, 3 L, 4 L and bulk) are labeled. b) AFM height image of the region inside the green square in (a). Inset: color bar of height signal. c) Height profile along the dashed line in (b). Inset: 3D plot of the AFM height signal. d) Photoluminescence and Raman spectra of sample S1. "1 L", "2 L", "3 L", and "4 L" indicate monolayer, bilayer, trilayer, and quadrilayer, respectively.

(2 L), trilayer (3 L), quadrilayer (4 L), and bulk (indicates thick layer) MoS_2 on a heavily doped p-type silicon wafer capped by a 285-nm-thick thermally grown silicon dioxide (SiO_2) layer. The number of the layers can be easily identified through the different optical contrasts, as shown in Figure 1a (the layer numbers are labeled). The height image obtained from a tapping-mode atomic force microscopy (AFM) measurement of the square region in Figure 1a (solid green lines) is shown in Figure 1b. A height profile along the dashed line in Figure 1b is depicted in Figure 1c, where the three-dimensional AFM height image is inserted. It is noted that the height of a monolayer MoS_2 on SiO_2 substrate is about 0.8–1.0 nm while that of a monolayer on MoS_2 flake is only 0.5–0.7 nm, consistent with the theoretical thickness of 6.15 Å.[17] The deviation could imply that the monolayer MoS_2 on SiO_2 substrate has absorbents on its surface so that it is thicker than the theoretical thickness.

Figure 1d depicts the photoluminescence (PL) and Raman spectra of sample S1 excited by 532 nm laser line at room temperature. One can see that the strongest PL signal is associated with monolayer MoS_2, while the bulk MoS_2 shows a negligible PL signal. The two PL peaks around 670 and 630 nm correspond to the A1 and B1 direct excitonic transitions at 1.85 and 1.97 eV, respectively.[18] It is worth noting that the PL signals of bilayer, trilayer, and quadrilayer MoS_2 are significantly weaker than that of monolayer MoS_2. The stronger PL emission in monolayer MoS_2 was attributed to much slower electronic relaxation arising from the unique electronic structure of monolayer MoS_2.[7] The very different PL spectra between monolayer and multilayer MoS_2 is consistent with the theoretical prediction that a monolayer MoS_2 is a direct bandgap material, while a multilayer MoS_2 is an indirect material.[7,8]

Figure 2a shows the Raman spectra of sample S1 excited by 488 nm line in air ambient environment. E^1_{2g} (~383 cm^{-1} for bulk MoS_2) and A_{1g} (~408 cm^{-1} for bulk MoS_2) modes are observed in both ultrathin and bulk MoS_2. (The E^2_{2g} mode is not detectable due to the constrain of our Rayleigh line rejection filter (>100 cm^{-1})). It is found that the frequency of E^1_{2g} peak decreases while that of the A_{1g} peak increases with increasing layer number. When the layer number increases, the interlayer Van der Waals force in MoS_2 suppresses atom vibration, resulting in higher force constants.[11] Thus, both E^1_{2g} and A_{1g} modes are supposed to stiffen (blue-shift). The observed blue-shift of A_{1g} peak with increasing layer number is consistent with the predicted stiffening. On the contrary, E^1_{2g} peak shows a red-shift, instead of a blue-shift, suggesting that the increased interlayer Van der Waals force plays a minor role while stacking-induced structure changes or long-range Coulombic interlayer interactions in multilayer MoS_2[15] may dominate the change of atomic vibration. Such thickness-dependent Raman spectra are found in more than a dozen of MoS_2 flakes with different layer numbers (see Figure S1 and S2a of the Supporting Information). Figure 2b shows the Raman mapping image with E^1_{2g} peak intensity using 488 nm laser line. It is noted that the contrast of the image with E^1_{2g} peak intensity is not uniform

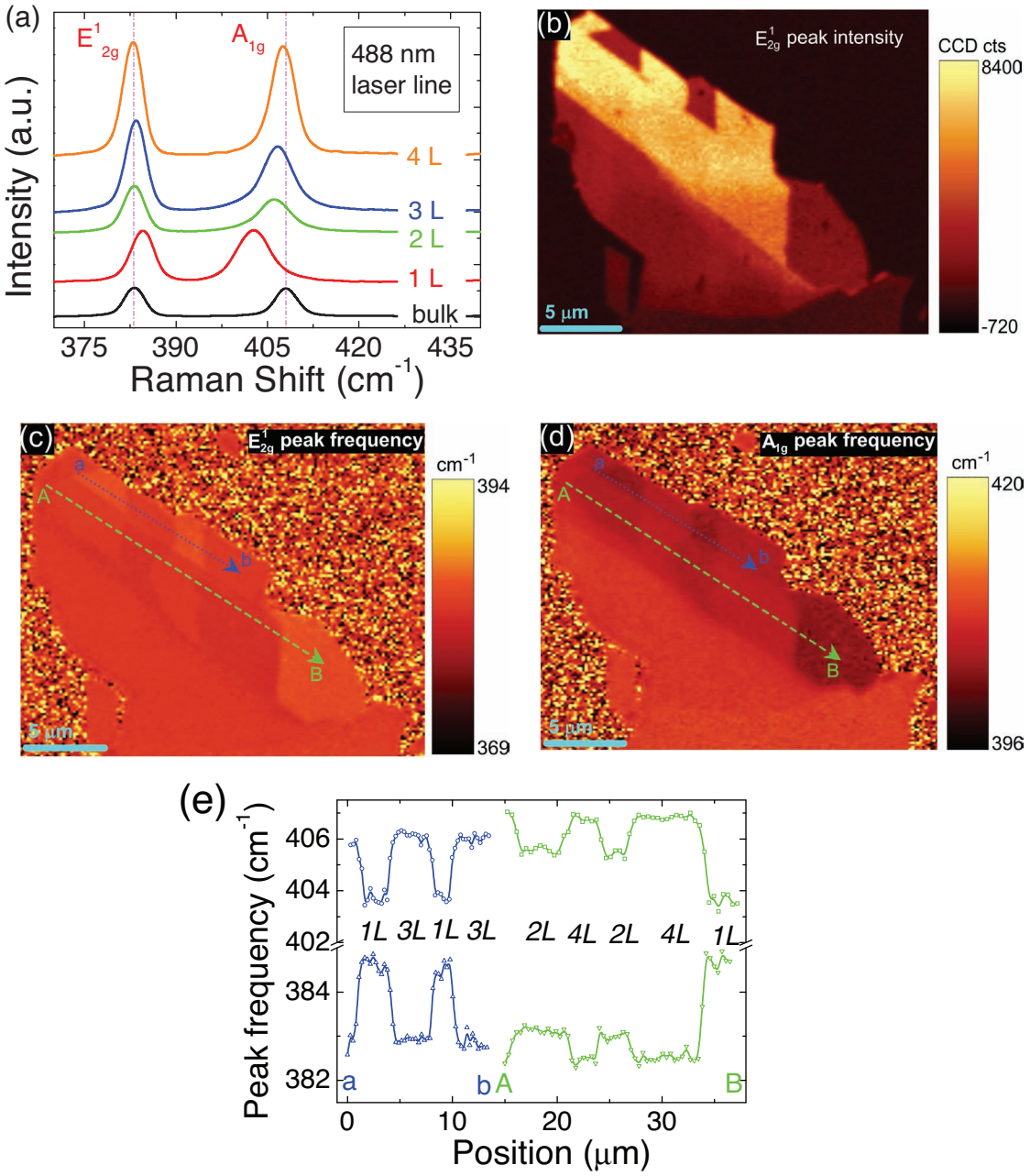

Figure 2. Raman characterizations of sample S1 using 488 nm laser line. a) Raman spectra of different locations with various thicknesses on sample S1. The left and right dashed lines indicate the positions of the E^1_{2g} and A_{1g} peaks in bulk MoS_2, respectively. b) Raman mapping image with the E^1_{2g} peak intensity, c) the E^1_{2g} peak frequency, and d) the A_{1g} peak frequency. Inset: color bars. The scale bars represent 5 μm. e) the E^1_{2g} and A_{1g} peak frequency profiles along the lines a–b and A–B drawn in (c) and (d). "1 L", "2 L", "3 L", and "4 L" indicate monolayer, bilayer, trilayer, and quadrilayer, respectively.

even in a region of a given thickness. It is even more difficult to differentiate layer numbers with E^1_{2g} peak width mapping (see Figure S2b of the Supporting Information). In addition, we were not able to distinguish layer numbers with A_{1g} peak intensity or width.

Figure 2c depicts the frequency mapping of E^1_{2g} peak (recorded simultaneously with those Raman images shown in Figure 2b), where the brighter color represents the blue-shift of E^1_{2g} peak. One can see that uniform color contrast in each region precisely corresponds to different thicknesses. It is noted that the brighter the color, the thinner the MoS_2 layer. The Raman frequency mapping of A_{1g} peak is shown in Figure 2d, where the darker color indicates the red-shift of A_{1g} peak. Figure 2e shows the frequency profiles of E^1_{2g} and A_{1g} peaks along the lines a–b and A–B drawn in Figures 2c and 2d. One can see that the frequency variation corresponds to the change in the layer number very well. The results are consistent with the aforementioned optical, AFM, and PL measurements.

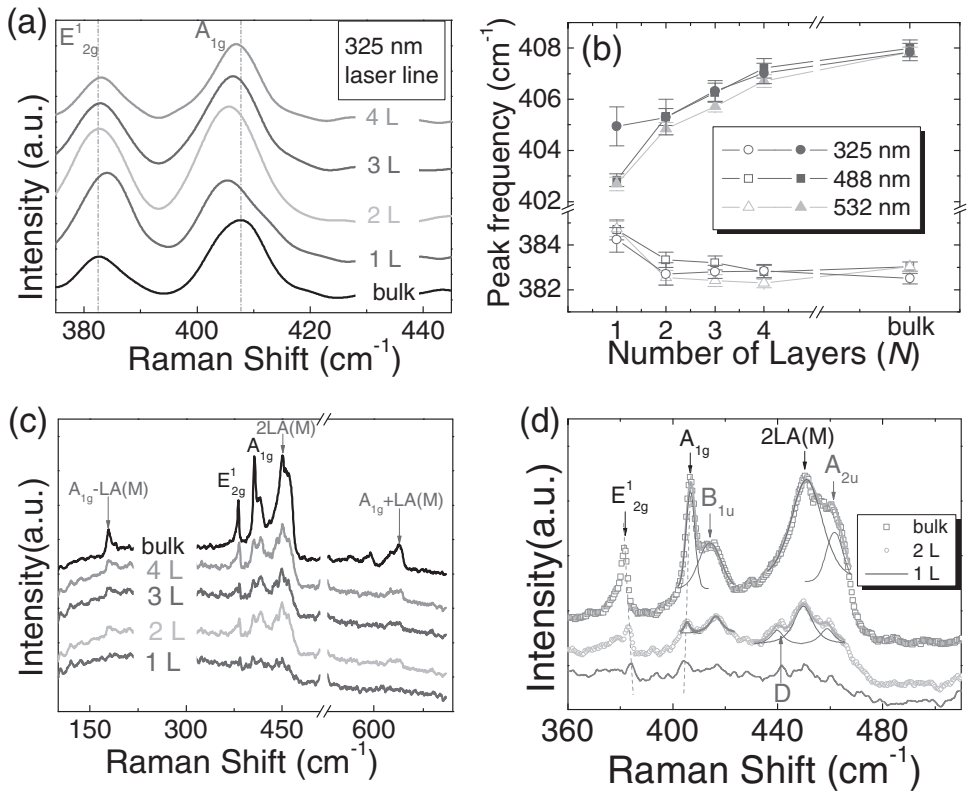

Figure 3. Raman characterizations of MoS_2 flakes using various lines. a) Raman spectra of various thicknesses on sample S1 using 325 nm lines. The left and right dashed lines indicate the positions of E^1_{2g} and A_{1g} peaks in bulk MoS_2, respectively. b) Thickness-dependent E^1_{2g} and A_{1g} peak frequencies using 325, 488, and 532 nm lines, respectively. c) Resonant Raman spectra using 632.8 nm line. d) Peak fitting on the resonant Raman spectra between 360 and 490 cm^{-1} of bilayer and bulk MoS_2. The solid lines are the fitting curves. The spectrum of monolayer MoS_2 is shown for comparison. "1 L", "2 L", "3 L", and "4 L" indicate monolayer, bilayer, trilayer, and quadrilayer, respectively.

Most importantly, the peak frequencies are uniform for a given thickness. These observations show that the E^1_{2g} and A_{1g} peak frequencies can be used to identify the layer number of an ultrathin MoS_2 flake with much higher accuracy than the intensities and widths of the peaks.

Figure 3a displays the Raman spectra of sample S1 excited by 325 nm line. The evident peak broadening could be caused by the low spectral resolution of the Raman spectroscopy with 325 nm laser. The frequencies of E^1_{2g} and A_{1g} peaks excited by 325, 488 and 532 nm laser lines are displayed in Figure 3b for comparison. Similar dependences of the peak frequencies on the layer number are observed (see Figure S2 for Raman spectra from more MoS_2 flakes). In obvious contrast, the Raman spectra excited by 632.8 nm line have more Raman peaks, as depicted in Figure 3c. On the spectrum of bulk MoS_2, the peaks around 180, 454, and 634 cm^{-1} are observed (besides the E^1_{2g} (382 cm^{-1}) and A_{1g} (407 cm^{-1}) peaks) owing to the resonance Raman (RR) scattering, because the 632.8 nm line is in resonance with the direct band gap (~1.96 eV) at the K point.[10,13,19] The assignment of the asymmetric peak centered at 454 cm^{-1} in bulk MoS_2 is an open question. It was previously assigned to the double frequency of the LA(M) mode (227 cm^{-1}).[10,19] Nevertheless, Frey et al. argue that it consists of two peaks, i.e., a second-order zone-edge phonon peak 2LA(M) and a first-order optical phonon peak A_{2u}.[20] A closer look in Figure 3d reveals that the asymmetric feature splits into three peaks around 440, 450, and 459 cm^{-1} in ultrathin MoS_2, providing a supportive evidence for Frey et al.'s argument. The Raman peak (D) at 440 cm^{-1} can be ascribed to Mo-S vibrations for oxysulfide species.[21,22] Oxygen may attack Mo–S–Mo bonds, especially at the edge of the flake, because of the existing dangling bonds. The oxygen-related peak appears only in ultrathin MoS_2 implies that oxygen is able to attack only surface layers. This finding indicates that passivation of monolayer/few-layer MoS_2 based optoelectronic devices is necessary to prevent oxygen from influencing device performances. Upon fitting, we obtain a LA(M) peak frequency of 226 cm^{-1} and A_{2u} peak frequency of 462 cm^{-1} (see Figure 3d). The peaks centered at 180 and 634 cm^{-1} are then assigned to $A_{1g}(M) - LA(M)$ and $A_{1g}(M) + LA(M)$ Raman modes, respectively.[19] Thus, the $A_{1g}(M)$ peak frequency is estimated as 407 ± 1 cm^{-1}, close to the $A_{1g}(\Gamma)$ peak frequency, consistent with the fact that the dispersion of A_{1g} mode in the $\Gamma - M$ direction is small.[14,23]

The intensity of A_{1g} peak is comparable with that of E^1_{2g} peak on the off-resonance spectra of sample S1 (see Figure 2a), whereas the intensity of A_{1g} peak is greatly enhanced with respect to that of E^1_{2g} peak under the resonance condition. The final state of direct electronic transition (K point) is mainly related to d^2_z orbitals of Mo atoms[24] that are aligned along the same direction (c axis) as the atomic displacements involved

in A_{1g} mode. Thus, a strong electron-phonon coupling along c axis is expected in RR scattering, resulting in the enhanced A_{1g} peak.[20] However, such an enhancement almost disappears in ultrathin MoS_2, indicating a weaker coupling between electronic transition at K point with A_{1g} phonon in ultrathin MoS_2 flakes. The weakened coupling could be ascribed to the increased transition energy at K point due to quantum confinement along the c axis[7,25] or elongated intralayer bonds in ultrathin MoS_2. The shoulder of A_{1g} peak in bulk MoS_2 evolves into an individual peak at 415 cm^{-1} in ultrathin MoS_2. This peak has been interpreted through a Raman-inactive mode (B_{1u}) due to a two-phonon scattering process involving a longitudinal quasi-acoustic phonon and a transverse optical phonon.[26] Both theoretical and experimental results suggest that the peak frequency of 415 cm^{-1} corresponds to an energy difference ΔE of 0.1 eV between the excitation laser energy (E_L) and that of A1 excitons (E_{A1}).[18] Thus, E_{A1} can be obtained as $E_L - \Delta E = 1.86$ eV, given E_L of 1.96 eV (632.8 nm). This estimation result agrees very well with A1 exciton energy of 1.85 eV obtained from PL measurement (see Figure 1d). Moreover, the deduced value of E_{A1} is comparable with 1.83 eV obtained by other group,[27] suggesting the validity of our assignment. The B_{1u} peak that forms a Davydov pair with A_{1g} peak appears due to the resonant effect.[23] The small frequency difference (7 cm^{-1}) between A_{1g} and B_{1u} peak indicates the weak interlayer interaction.[26] Similar observations are found in different MoS_2 flakes, as shown in Figure S3 of the Supporting Information.

The Raman spectra of sample S2 (see inset for the optical image) excited by 532 nm laser line are depicted in **Figure 4**a. In comparison with sample S1, sample S2 is so small that it is difficult to resolve the different thicknesses using optical microscopy with the 100× objective. Interestingly, the Raman mapping images give a higher resolution than the optical images, as shown in Figures 4b and c. Regions with different layer numbers are unambiguously distinguished by clear boundaries. The E^1_{2g} and A_{1g} peak frequencies measured using different laser lines are summarized in **Table 1**. As the layer number increases, two notable features can be seen: 1) a red-shift about 2.2 cm^{-1} (standard deviation of 0.7) is associated with the E^1_{2g} peak, and 2) a blue-shift of 4.1 cm^{-1} (standard deviation of 1.0) is observed for the A_{1g} peak. Moreover, the E^1_{2g} and A_{1g} peak frequencies of 384.6 cm^{-1} (standard deviation of 0.3) and 403.4 cm^{-1} (standard deviation of 0.5) are obtained for monolayer MoS_2. The small deviation values imply that Raman spectroscopy could serve as a reliable tool for identifying monolayer MoS_2.

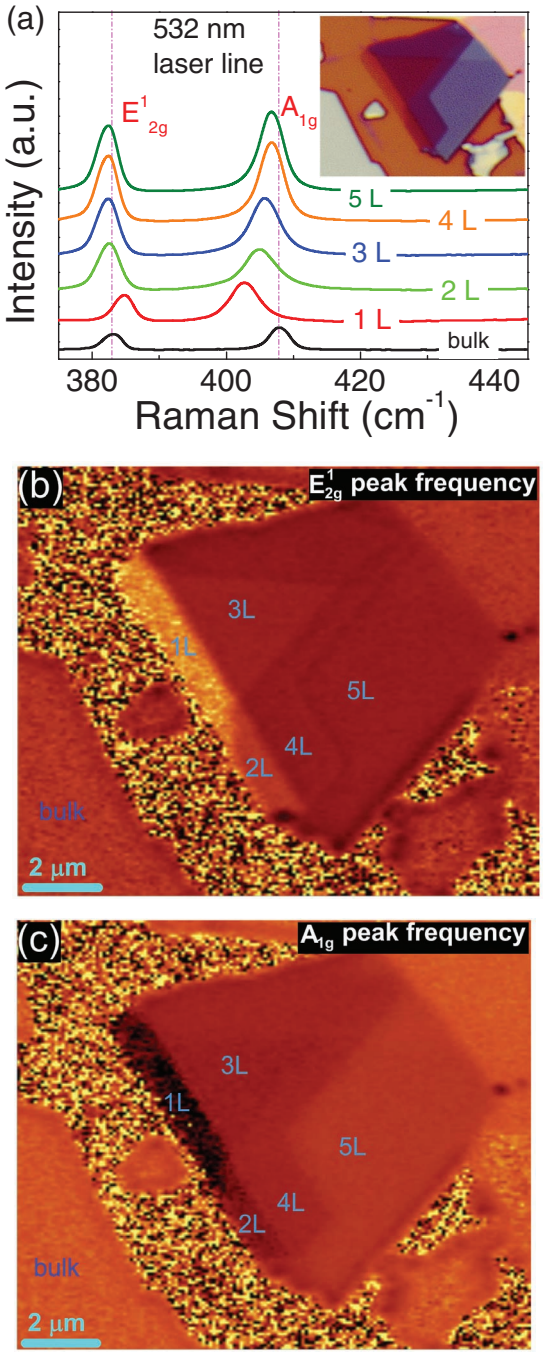

Figure 4. Raman characterizations of sample S2 using 532 nm line. a) The Raman spectra of different locations with various thicknesses on sample S2. Inset: optical image of sample S2. The left and right dashed lines indicate the positions of the E^1_{2g} and A_{1g} peaks in bulk MoS_2, respectively. Raman mapping image with (b) the E^1_{2g} peak frequency and (c) the A_{1g} peak frequency. The scale bars represent 2 μm. "1 L", "2 L", "3 L", "4 L", and "5 L" indicate monolayer, bilayer, trilayer, quadrilayer, and quinquelayer, respectively.

3. Conclusions

Ultrathin MoS_2 flakes have been investigated systematically using Raman and resonance Raman spectroscopy. The frequencies, widths and intensities of the Raman E^1_{2g} and A_{1g} peaks are strongly influenced by the thicknesses of the ultrathin flakes. However, only the frequencies of E^1_{2g} and A_{1g} peaks can be used as key features to identify the layer number of a MoS_2 flake (≤4 layers). The layer number identification using E^1_{2g} or A_{1g} peaks frequency are consistent with optical, AFM and PL characterization. Resonance Raman spectra show that the coupling between electronic transition at K point and A_{1g} phonon is weakened in ultrathin MoS_2 in comparison with that in bulk MoS_2, which is ascribed to the increased transition energy at K point due to the perpendicular quantum confinement or elongated intralayer atomic bonds. We confirm that

Table 1. Summary of the E^1_{2g} and A_{1g} peak frequencies with various laser lines. "1 L", "2 L", "3 L", and "4 L" indicate monolayer, bilayer, trilayer, and quadrilayer, respectively. A single data represents the average value from three different samples. The measurement results with 514.5 nm line are extracted from reference [15].

Laser lines [nm]	E^1_{2g} peak frequency [cm^{-1}]					A_{1g} peak frequency [cm^{-1}]				
	1 L	2 L	3 L	4 L	bulk	1 L	2 L	3 L	4 L	bulk
325	384.2	382.8	382.8	382.7	382.5	404.9	405.5	406.3	407	407.8
488	384.7	383.3	383.2	382.9	383	402.8	405.5	406.5	407.4	408
514.5[15]	384.3	383.2	382.7	382.3	382	403	404.8	405.8	406.7	407.5
532	384.7	382.5	382.4	382.4	383	402.7	404.9	405.7	406.7	407.8
632.8	385	383.8	383.3	382.9	381.5	403.8	404.8	405	406	406.6

the asymmetric Raman feature centered at 454 cm^{-1} in bulk MoS_2 is actually a combinational band involving LA(M) and A_{2u} modes. The consistent E^1_{2g} and A_{1g} peak frequencies of monolayer MoS_2 using various laser lines show that Raman spectroscopy is a reliable diagnostic tool to identify monolayer MoS_2.

4. Experimental Section

MoS_2 flakes were mechanically exfoliated from a piece of commercially available nature crystalline MoS_2 sample (SPI Supplies) with Scotch tape. The Raman measurements with the excitation laser lines of 488, 532 and 632.8 nm were performed using a WITEC alpha300 R Confocal Raman system in air ambient environment. The Raman measurements with the excitation laser line of 325 nm were performed using a Renishaw Raman spectroscopy integrated with a Kimmon IK5751I-G UV laser. The powers of the excitation laser lines are kept well below 1 mW to avoid heating effect. The Raman emission was collected by an Olympus 100× objective (N.A. = 0.8) and dispersed by 600 (for PL measurement in Figure 1d and resonance Raman measurement in Figure 3c and d), 1800 (for Raman measurement in Figure 2 and 4) and 2400 (Figure 3a) lines mm^{-1} gratings. The Renishaw Raman spectroscopy with 325 nm line and 2400 lines mm^{-1} grating has a step size of 3–4 cm^{-1}. The WITEC Raman spectroscopy with 600 lines mm^{-1} grating has a spectral resolution around 2 cm^{-1} while that with 1800 lines mm^{-1} grating has a spectral resolution better than 1 cm^{-1}.

Supporting Information

Supporting Information is available from the Wiley Online Library or from the author.

Acknowledgements

This work was supported by Temasek Laboratory and Ministry of Education of Singapore.

Received: September 6, 2011
Published online: January 31, 2012

[1] E. Fortin, W. M. Sears, *J. Phys. Chem. Solids* **1982**, *43*, 881.
[2] E. Gourmelon, O. Lignier, H. Hadouda, G. Couturier, J. C. Bernède, J. Tedd, J. Pouzet, J. Salardenne, *Sol. Energy Mater. Sol. Cells* **1997**, *46*, 115.
[3] W. Ho, J. C. Yu, J. Lin, J. Yu, P. Li, *Langmuir* **2004**, *20*, 5865.
[4] K. S. Novoselov, A. K. Geim, S. V. Morozov, D. Jiang, Y. Zhang, S. V. Dubonos, I. V. Grigorieva, A. A. Firsov, *Science* **2004**, *306*, 666.
[5] B. Radisavljevic, A. Radenovic, J. Brivio, V. Giacometti, A. Kis, *Nat. Nanotechnol.* **2011**, *6*, 147.
[6] Y. Yoon, K. Ganapathi, S. Salahuddin, *Nano Lett.* **2011**, *11*, 3768.
[7] A. Splendiani, L. Sun, Y. Zhang, T. Li, J. Kim, C.-Y. Chim, G. Galli, F. Wang, *Nano Lett.* **2010**, *10*, 1271.
[8] K. F. Mak, C. Lee, J. Hone, J. Shan, T. F. Heinz, *Phys. Rev. Lett.* **2010**, *105*, 136805.
[9] J. L. Verble, T. J. Wieting, *Phys. Rev. Lett.* **1970**, *25*, 362.
[10] J. M. Chen, C. S. Wang, *Solid State Commun.* **1974**, *14*, 857.
[11] A. G. Bagnall, W. Y. Liang, E. A. Marseglia, B. Welber, *Physica* **1980**, *99B*, 343.
[12] M. Viršek, A. Jesih, I. Milošević, M. Damnjanović, M. Remškar, *Surf. Sci.* **2007**, *601*, 2868.
[13] B. C. Windom, W. G. Sawyer, D. W. Hahn, *Tribol. Lett.* **2011**, *42*, 301.
[14] P. A. Bertrand, *Phys. Rev. B* **1991**, *44*, 5745.
[15] C. Lee, H. Yan, L. E. Brus, T. F. Heinz, J. Hone, S. Ryu, *ACS Nano* **2010**, *4*, 2695.
[16] H. Li, Q. Zhang, C. Liu, S. Xu, P. Gao, *ACS Nano* **2011**, *5*, 3198.
[17] R. F. Frindt, *J. Appl. Phys.* **1966**, *37*, 1928.
[18] T. Livneh, E. Sterer, *Phys. Rev. B* **2010**, *81*, 195209.
[19] A. M. Stacy, D. T. Hodul, *J. Phys. Chem. Solids* **1985**, *46*, 405.
[20] G. L. Frey, R. Tenne, M. J. Matthews, M. S. Dresselhaus, G. Dresselhaus, *Phys. Rev. B* **1999**, *60*, 2883.
[21] G. L. Schrader, C. P. Cheng, *J. Catal.* **1983**, *80*, 369.
[22] E. Payen, S. Kasztelan, S. Houssenbay, R. Szymanski, J. Grimblot, *J. Phys. Chem.* **1989**, *93*, 6501.
[23] T. Sekine, M. Izumi, T. Nakashizu, K. Uchinokura, E. Matsuura, *J. Phys. Soc. Jpn.* **1980**, *49*, 1069.
[24] R. Coehoorn, C. Haas, R. A. de Groot, *Phys. Rev. B* **1987**, *35*, 6203.
[25] H. S. S. Ramakrishna Matte, A. Gomathi, A. K. Manna, D. J. Late, R. Datta, S. K. Pati, C. N. R. Rao, *Angew. Chem.* **2010**, *122*, 4153.
[26] T. Sekine, K. Uchinokura, T. Nakashizu, E. Matsuura, R. Yoshizaki, *J. Phys. Soc. Jpn.* **1984**, *53*, 811.
[27] C. H. Ho, C. S. Wu, Y. S. Huang, P. C. Liao, K. K. Tiong, *J. Phys.: Condens. Matter* **1998**, *10*, 9317.